Tracking of geoacoustic parameters using Kalman and particle filters

Caglar Yardim,[a] Peter Gerstoft,[b] and William S. Hodgkiss[c]
Marine Physical Laboratory, Scripps Institution of Oceanography, La Jolla, California 92093-0238

(Received 9 June 2008; revised 14 November 2008; accepted 20 November 2008)

This paper incorporates tracking techniques such as the extended Kalman, unscented Kalman, and particle (PF) filters into geoacoustic inversion problems. This enables spatial and temporal tracking of environmental parameters and their underlying probability densities, making geoacoustic tracking a natural extension to geoacoustic inversion techniques. Water column and seabed properties are tracked in simulation for both vertical (VLA) and horizontal (HLA) line arrays using the three tracking filters. Filter performances are compared in terms of filter efficiencies using the posterior Cramér–Rao lower bound. Tracking capabilities of the geoacoustic filters under slowly and quickly changing environments are studied in terms of divergence statistics. Geoacoustic tracking can provide continuously environmental estimates and their uncertainties using only a fraction of the computational power of classical geoacoustic inversion schemes. Interfilter comparison show that while a high-particle-number PF outperforms the Kalman filters, there are many cases where all three filters perform equally well depending on the inversion configuration (such as the HLA versus VLA and frequency) and the tracked parameters.
 [DOI: 10.1121/1.3050280]

PACS number(s): 43.30.Pc, 43.60.Pt, 43.60.Wy [AIT] Pages: 746–760

I. INTRODUCTION

Geoacoustic inversion is a technique used to extract information about the ocean environment by analyzing the acoustical field propagation in that medium. Typically, water column and seabed parameters such as sound speed profiles (SSPs), sediment densities, layer thicknesses, and attenuations are estimated by finding an environmental model that generates an acoustic field that matches closely the measured field. There are different configurations that are typically used in geoacoustic inversion, each with its own advantages and drawbacks. Some of the most commonly used ones include vertical (VLA) or horizontal (HLA) line arrays, bottom moored or towed arrays, and active or passive source configurations that use either a separate towed source or ship self-noise for inversion.[1–7] While some of the inversion techniques focus on obtaining the optimum solution with minimum computation time using efficient global optimizers such as genetic algorithms[8] or simulated annealing,[9] the others estimate the probability densities of the environmental parameters to compute the uncertainty in the estimated parameters.[10,11] This enables them to project this environmental uncertainty into parameters-of-interest such as the uncertainties in transmission loss and statistical sonar performance prediction.[12]

This paper reformulates the geoacoustic inversion algorithms that estimate the geoacoustic environment between the source and the receiver array at a given time into tracking the evolution of these parameters and their associated uncertainties in space and time. This is achieved by merging geoacoustic inversion techniques with tracking algorithms such as the Kalman and particle filters (PFs). These filters have been used previously in estimation[13] and temporal tracking[14] of the ocean SSP and similar acoustic applications.[15,16]

Here, the geoacoustic tracking problem is formulated in a Kalman framework, and depending on the source/receiver configuration, the acoustic field is calculated using either the normal mode code SNAP (Ref. 17) or the complex normal mode code ORCA (Ref. 18) for near-field calculations. This interaction between the environmental parameters and the acoustic field can involve a high level of nonlinearity. In addition, it is known from previous studies[19–21] that the posterior probability densities (PPDs) of geoacoustic parameters can be non-Gaussian. Therefore, geoacoustic tracking is a challenging task and requires tracking filters that can handle nonlinear, non-Gaussian systems. This paper studies the suitability of three such filters, namely, the extended Kalman filter[22] (EKF), the unscented Kalman filter[23] (UKF), and the PF (Ref. 24) in geoacoustic tracking. All three filters use different schemes to deal with such complex systems. The EKF extends the best possible filter in a linear/Gaussian system, i.e., the Kalman filter (KF), into the nonlinear/non-Gaussian domain by analytical linearization of the problem. Instead, the UKF uses statistical linearization with unscented transform. Finally, the PF propagates a large number of particles to represent the evolving probability density function (PDF) of the environmental parameters. In this paper, the tracked parameters are restricted to environmental parameters since detection and tracking of a target/source using tracking filters are already well-studied fields in applications involving sonar and radars.

Most cases that require consecutive geoacoustic inversions to obtain the spatial/temporal variation of geoacoustic parameters effectively can be reformulated as tracking prob-

[a]Electronic mail: cyardim@ucsd.edu
[b]Electronic mail: gerstoft@ucsd.edu
[c]Electronic mail: whodgkiss@ucsd.edu

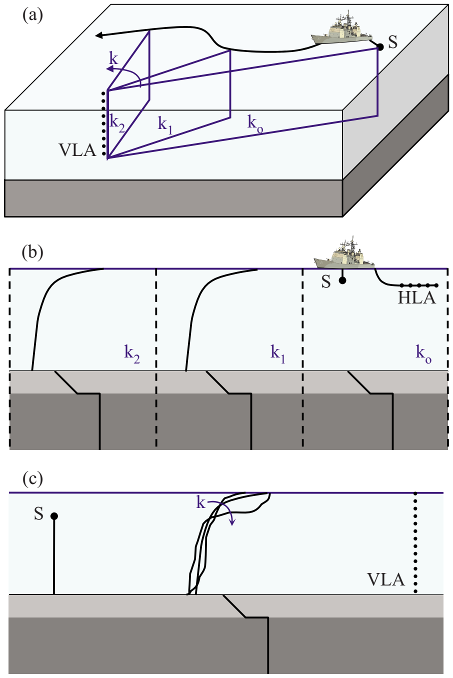

FIG. 1. (Color online) Geoacoustic tracking for three configurations: (a) Temporal tracking of the average, range-independent environment using a fixed-VLA-receiver and a towed-source, (b) spatial tracking of range-dependence using a towed-HLA-receiver and a towed-source, and (c) temporal tracking of the ocean sound speed profile for a fixed-VLA-receiver and a fixed-source.

lems. Three examples are shown in Fig. 1:

(a) Figure 1(a) shows a typical fixed hydrophone array (VLA or HLA) configuration and a separate towed source with the aim of capturing the environment between the moving source and the receiver array. The two dimensional environment between the source and the array changes as the source is towed, resulting in an evolution of the range-independent model in time, as shown in the figure as step indices k_i. For example, such a scenario could transform the following geoacoustic inversion approaches into geoacoustic tracking:
   - a towed source and fixed VLA [e.g., SWARM'95 (Ref. 21)],
   - a towed source and fixed HLA [e.g., SWAMI'98 (Ref. 2) and Barents Sea'03 (Ref. 6)],
   - the test cases used in the Geoacoustic Inversion Techniques Workshop with a moving source and fixed HLA (Ref. 25), and
   - a single hydrophone mounted on seafloor receiving transmission from a towed source [e.g., SCARAB'98 (Ref. 26)].

(b) Figure 1(b) represents the type of configuration that is designed to capture range-dependent environmental parameters at small range increments. The illustration given in the figure uses a HLA and a source close to the array, both towed by the same ship. Hence, the HLA captures the near-field acoustic field that is affected only by a small section of the water column and seabed. It is possible to take each of these sections as a step index in range and assume that the environment is constant within each k_i, and therefore turn it into a range-dependent environment tracking problem. The update rate can be increased using overlapping blocks but for the sake of simplicity, a nonoverlapping scheme is shown here. This type of geoacoustic tracking could be used in
   - a towed source and HLA [e.g., MAPEX2000 (Refs. 1, 5, and 7)],
   - tow-ship self-noise data acquired via a towed HLA [e.g., MAPEX2000 (Ref. 3)], and
   - passive fathometer using the ocean ambient noise field measured by a drifting VLA [e.g., ASCOT'01 and Boundary'03 (Ref. 27)].

(c) The last example, given in Fig. 1(c), estimates the evolution in time of the water column SSP along a fixed path. Such a scenario could be implemented in the following examples:
   - a fixed source and fixed VLA [e.g., Yellow Shark'94 (Ref. 28)] and
   - KFs used to track the SSP in a similar configuration during the MREA/BP'07 experiment (Ref. 14)

The main objective of this paper is to incorporate tracking filters into the geoacoustic inversion problem and test the effectiveness of each filter in geoacoustic parameter tracking.

II. GEOACOUSTIC ESTIMATION AS A TRACKING PROBLEM

Geoacoustic inversion requires a measurement equation relating the simulated acoustic field to the observed data through a forward model. This is represented using[10,11]

$$\mathbf{d}^{\mathrm{obs}} = s\mathbf{d}(\mathbf{m}) + \mathbf{e}, \tag{1}$$

where $\mathbf{d}^{\mathrm{obs}}$ represents the complex-valued acoustic data vector along the array, s is the complex source magnitude, $\mathbf{d}(\mathbf{m})$ is the simulated field obtained using the acoustic propagation model for an environment represented by the environmental model vector $\mathbf{m}$, and $\mathbf{e}$ is complex Gaussian noise. Using Eq. (1), a geoacoustic inversion algorithm defines an objective function to be used in the inversion to obtain the best possible model $\hat{\mathbf{m}}$.

Geoacoustic tracking, on the other hand, uses two dynamic equations to characterize the system:

- An equation modeling the evolution of the environmental model parameters governed by the physical processes in the medium such as ocean currents and mixing, bathymetry, and the expected rate of change in seabed parameters in range.
- An acoustic measurement equation similar to Eq. (1). However, this is a dynamic equation that includes a continuous stream of data $\mathbf{d}_k^{\mathrm{obs}}$, where k represents the temporal or spatial step index.

Following standard KF notation,[29] the error $\mathbf{e}$ in the measurement equation, the environmental model $\mathbf{m}$, and the acoustic field across the hydrophone array $\mathbf{d}^{\mathrm{obs}}$ at step k henceforth will be denoted by $\mathbf{w}_k$, $\mathbf{x}_k$, and $\mathbf{y}_k$, respectively. Therefore, the set of equations at step k are

$$\mathbf{x}_k = \mathbf{f}(\mathbf{x}_{k-1}) + \mathbf{v}_{k-1}, \tag{2}$$

$$\mathbf{y}_k = \mathbf{h}(\mathbf{x}_k) + \mathbf{w}_k = s_k \mathbf{d}(\mathbf{x}_k) + \mathbf{w}_k, \tag{3}$$

where $\mathbf{f}(\cdot)$ is a known function of the state vector $\mathbf{x}_{k-1}$, and $\mathbf{h}(\cdot)$ is the nonlinear function that relates the environmental parameters $\mathbf{x}_k$ to the acoustic measurement vector $\mathbf{y}_k$. Hence, $\mathbf{h}(\cdot)$ includes both the unknown source term s_k and the known forward model $\mathbf{d}(x_k)$ as given in Eq. (1). $\mathbf{v}_k$ and $\mathbf{w}_k$ are the process/state and the measurement noise vectors, respectively, with

$$E\{\mathbf{v}_k \mathbf{v}_i^T\} = \mathbf{Q}_k \delta_{ki},$$

$$E\{\mathbf{w}_k \mathbf{w}_i^T\} = \mathbf{R}_k \delta_{ki},$$

$$E\{\mathbf{v}_k \mathbf{w}_i^T\} = \mathbf{0}, \quad \forall\, i,k, \tag{4}$$

where $\mathbf{Q}_k$ and $\mathbf{R}_k$ are the covariance matrices at time k of the corresponding noise terms. Similar to geoacoustic inversion, the state vector $\mathbf{x}_k$ is composed of the n_x parameters that describe the environment at step k. In geoacoustic tracking, however, these model parameters also evolve so the algorithm continuously updates the best estimate and the uncertainties in these estimates.

Equation (2) is the state equation modeling the evolution of the environmental parameters. Any prior knowledge about the environment and its evolution are modeled here. The values of the environmental parameters at step k are related to their values in the previous step $k-1$ by the function $\mathbf{f}(\cdot)$. If the environmental model evolution is linear, $\mathbf{f}(\cdot)$ can be modeled by the matrix $\mathbf{F}$, which is assumed in this paper. This assumption is reasonable if the parameter update rate is higher than the rate of change in the environment. The process noise $\mathbf{v}_k$ is a function of how correctly the evolution is modeled, which is usually taken as a zero-mean Gaussian PDF, allowing the filter to capture the changes per step that are not included in the evolution model. For example, the geoacoustic parameters are assumed to vary slowly with $\mathbf{F} = \mathbf{I}_{n_x \times n_x}$. Even though many geoacoustic parameters such as the sediment layer thickness may satisfy this condition most of the time, there can be sudden jumps at the boundaries of geological formations, violating the evolution model selected here. To continue tracking the parameters successfully through the sudden jump, the geoacoustic tracking filters will have to incorporate a state noise term with a high covariance $\mathbf{Q}_k$. The initial density $p(\mathbf{x}_0)$ can be obtained by running a Markov chain Monte Carlo geoacoustic inversion at $k=0$.

Equation (3) is the measurement equation relating the environmental model parameters to acoustic measurements. This process involves the selection of a suitable forward model that propagates acoustic fields and simulates the field observed across the receiver array for a given environmental model. The forward model is selected, taking into account the complexity of the model chosen to represent the environment, the selection of the source and receiver array configurations, and the available computational power. The most commonly used propagation models are normal mode (complex versions when the near-field is needed, adiabatic versions for mildly range-dependent configurations), ray tracing, and parabolic equation (using either split-step fast Fourier transform or Padé coefficients). SNAP is used here with the long-range VLA configuration, and complex ORCA is used with the near-field HLA simulations. The noise term is assumed complex Gaussian with covariance $\mathbf{R}_k$ obtained from the array signal-to-noise ratio (SNR) [see Eq. (9)]. Since the synthetic data used here are generated using the same forward model and environmental parameters, there is no modeling error in the examples. Working with real data will include unavoidably the modeling uncertainty, resulting in an increase in the noise term.

The KFs necessitate a linear/Gaussian framework, whereas any distribution can be used for the PF. This means that the prior PDF $p(\mathbf{x}_0)$, the state variables, state, and measurement noise all have to be Gaussian to run any KF algorithm as a geoacoustic tracking filter. PFs can work with any PDF. However, in order to compare these two types of filters under identical initial conditions, the prior densities at $k=0$ are taken as Gaussian PDF in this paper. The results of the KFs will all be Gaussian, while the PF densities can be of any distribution.

III. THEORY

For a system with linear state and measurement equations and Gaussian PDFs the KF (Ref. 22) is the optimal filter in a minimum mean square error (MSE) sense. However, for nonlinear, non-Gaussian problems such as geoacoustic tracking, it may not be possible to find an optimal estimator. Therefore, three suboptimal filters are investigated:

- EKF that uses analytical linearization where the measurement equation is linearized using the first order Taylor series expansion,
- UKF that uses statistical linearization where the nonlinearity in the parabolic equation is kept but PDFs are restricted to be Gaussian, and
- PF or sequential Monte Carlo (SMC), which uses a sequential importance resampling (SIR) or bootstrap filter to track the nonlinear, non-Gaussian system.

Each of these algorithms has their advantages and drawbacks for different tracking applications. See Appendix A for filter descriptions and implementation details.

The filters can be compared to each other using the root mean square (RMS) error between the true environment $\mathbf{x}_k$ and the filter estimate $\hat{\mathbf{x}}_{k|k}$. However, this only shows if one filter is doing better than the others, giving no indication about whether and to what extent the information available through previous states and current measurements are exploited by the filter, especially given the fact that all three of these filters are suboptimal. Therefore, it is desirable to have a tool that can not only assess the performances of these techniques but also provide a limit to achievable performance for a given environment.

This is done by using the posterior or Bayesian Cramér–Rao lower bound (PCRLB) introduced by van Trees[30] (see Appendix B). PCRLB is the Bayesian counterpart of the classical Cramér-Rao lower bound (CRLB) defined in a non-Bayesian framework as the inverse of the Fisher information matrix. There are studies on the calculation of both the CRLB (Ref. 31) and the PCRLB (Ref. 32) for geoacoustic inversion problems. Any filter that achieves a MSE equal to the PCRLB is called an efficient estimator. For a linear and Gaussian system, the KF is an efficient estimator. It may not be possible to attain the PCRLB for a nonlinear, non-Gaussian system.

The performance metrics used in this paper are

$$\mathrm{RMS}_k(i) = \left[\sum_{j=1}^{n_{\mathrm{MC}}} \frac{(\hat{\mathbf{x}}_k^j(i) - \mathbf{x}_k^j(i))^2}{n_{\mathrm{MC}}} \right]^{1/2}, \tag{5}$$

$$\eta_k(i) = \mathbf{J}_k^{-1/2}(i,i)/\mathrm{RMS}_k(i), \tag{6}$$

$$\mathrm{RTAMS}(i) = \left[\sum_{k=k_1}^{k_2} \sum_{j=1}^{n_{\mathrm{MC}}} \frac{(\hat{\mathbf{x}}_k^j(i) - \mathbf{x}_k^j(i))^2}{(k_2 - k_1 + 1)n_{\mathrm{MC}}} \right]^{1/2}, \tag{7}$$

$$\mathrm{Improv} = \frac{\mathrm{RTAMS}_{\mathrm{EKF}} - \mathrm{RTAMS}_{\mathrm{filter}}}{\mathrm{RTAMS}_{\mathrm{EKF}}}, \tag{8}$$

where $\mathbf{x}_k^j(i)$ is the ith parameter of the true state vector $\mathbf{x}$ at time index k for the jth MC run, RMS_k, $\mathbf{J}_k$, and η_k are the root mean square error, the Fisher information matrix (inverse of the PCRLB), and the filter efficiency, respectively, at step k. RTAMS is the root time averaged mean square error[29] calculated for the interval $[k_1, k_2]$, and Eq. (8) calculates the performance improvement of a filter with respect to the EKF.

IV. EXAMPLES

This section is composed of three geoacoustic tracking examples that either spatially or temporally track the evolving environment and the PPD. The first two use the configuration in Fig. 1(a), and the last one uses the one in Fig. 1(b). The simulation parameters such as the array structure, water depth, and source frequencies are selected similar to the ones that are used in Refs. 1 and 20. Each example evaluates and compares different aspects of the tracking algorithms. These three examples are

(1) Temporal tracking. Filter efficiencies, PCRLB calculations, performance limitation analysis, computational costs, effects of increasing the particle size in PF, and interfilter comparison of uncertainty propagation are studied using temporal tracking of an effective range-independent environment (with n_x=4 unknown parameters at each step k).
(2) Divergence analysis. For both slowly varying and abruptly changing environments, a divergence analysis is carried out using n_x=7 unknown parameters at each step k.
(3) Spatial tracking. The effects of selection of geoacoustic setup on filters and tracking performance of individual geoacoustic parameters are investigated using spatial tracking of a range-dependent environment represented by n_x=7 unknown parameters at each spatial step k.

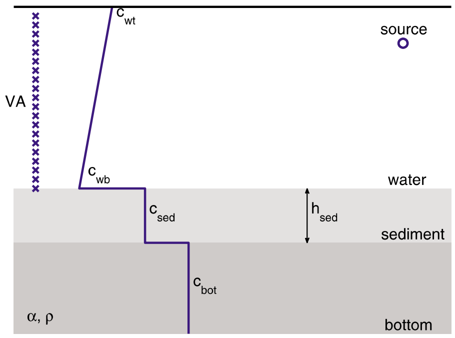

FIG. 2. (Color online) Seven-parameter geoacoustic model used in the simulations.

A. Example 1: Temporal tracking using a VLA

This example compares the performance of the EKF, UKF, and PF with the best possible limit given by the PCRLB in terms of the RMS error and the filter efficiency. The range-independent environment model used is given in Fig. 2. Note that the selection of the environmental model is arbitrary, and multiple more complex models can be incorporated into filters such as the multiple model particle filter (MMPF).[29]

Only the four parameters representing the sediment layer, namely, sound speed, thickness, attenuation, and density, are tracked in this example. A sandy silt with medium-fine to fine sand sediment is used in the tracking.[7] A VLA spanning the entire 100 m water column with 20 hydrophones is used. A frequency of 250 Hz is selected. All the environmental constants, state variables, their initial means and covariances, and the filter parameters are given in Table I. The covariance of the measurement error term $\mathbf{R} = \nu \mathbf{I}$ is computed from the array SNR (Ref. 20) defined as

$$\mathrm{SNR} = 10 \log \frac{[s\mathbf{d}(\mathbf{x})]^H [s\mathbf{d}(\mathbf{x})]}{\nu}. \tag{9}$$

The PCRLB and the filter performances are calculated using the Monte Carlo (MC) analysis as discussed in Appendix B. First, n_{MC}=100 evolving environments (each one a MC trajectory) are created using the state equation, with starting values selected from a Gaussian with a mean of $\mathbf{x}_0$ and covariance $\mathbf{P}_0$. These trajectories are given in Fig. 3(a). Then the PCRLB is computed using Eq. (B2) where the first term ($\mathbf{D}_{k-1}^{22}$) is estimated using Eq. (B8). Each of these 100 trajectories is also tracked by the EKF, UKF, and PFs using 200, 2000, and 10 000 particles designated by PF-200, PF-2000, and PF-10 000, respectively. The normal mode code SNAP is selected as the forward model.

The evolution of the RMS error in Eq. (5) of each parameter is computed for each filter and is given in Fig. 3(b) as a function of step index k. Note that the region below the square root of the PCRLB is shaded as unobtainable RMS values. Also note that the filter RMS error estimates can initially get lower than this limit before they increase and stabilize to their real values. Hence, this region is discarded in the calculations by setting the $[k_1, k_2]$ interval as $[100, 150]$ min for the RTAMS in Eq. (7) and their following improvement-over-EKF computations in Eq. (8).

TABLE I. Environmental and simulation parameters used in example 1.

Environment					
		State variables			
Constants		$\mathbf{x}$	$E[\mathbf{x}_0]$	$\mathbf{P}_0^{1/2}$	State noise ($\mathbf{Q}_k^{1/2}$)
c_{wt}	1480 m/s	c_{sed} (m/s)	1600	1	0.35
c_{wb}	1460 m/s	h_{sed} (m)	15	0.5	0.35
h_w	100 m	α_{sed} (dB/λ)	0.25	0.01	0.0015
c_{bot}	1700 m/s	ρ_{sed} (g/cm^3)	1.8	0.1	0.03
Simulation parameters					
Source depth		20 m	Source frequency		250 Hz
Source range		5 km	Array SNR ($\mathbf{R}_k$)		40 dB
Receiver type		VLA	Track length		2.5 h (k=30)
No. of hydrophones		20	Track frequency		1 measurement/5 min
Array start, Δz		5 m, 5 m	MC runs		100

The results given in Fig. 3(b) show that the PFs perform better than the EKF and the UKF. While sediment thickness and sound speed tracking using PF is clearly superior to the KF variants, only PF with a large number of particles outperforms the EKF and UKF tracking of the sediment density, and all three types of filters perform well for attenuation tracking, closely following the theoretical limit set by the PCRLB. The RMS errors in sediment parameters, the average efficiency after 2.5 h of tracking, RTAMS values, and improvement-over-EKF percentages are given in Table II. Due to its inherent limitations, the EKF achieves an average filter efficiency of 52%. The UKF performs only slightly better with a 2% improvement over the EKF. With an efficiency of 63%, the PF-200 is 19% better than the EKF. Increasing the particle number improves performance to 80% efficiency in the PF-2000. The PF-10 000 results show that further increase in the particle number does not result in an increase in the performance, with a 37% improvement over the EKF out of a theoretical upper limit of 48% dictated by the PCRLB. PF-10 000 results are not shown in Fig. 3(b) but are given in Table II.

Even though PF performs better than the KFs in terms of RMS errors, it is also important to compare the computational cost of each algorithm both with each other and with

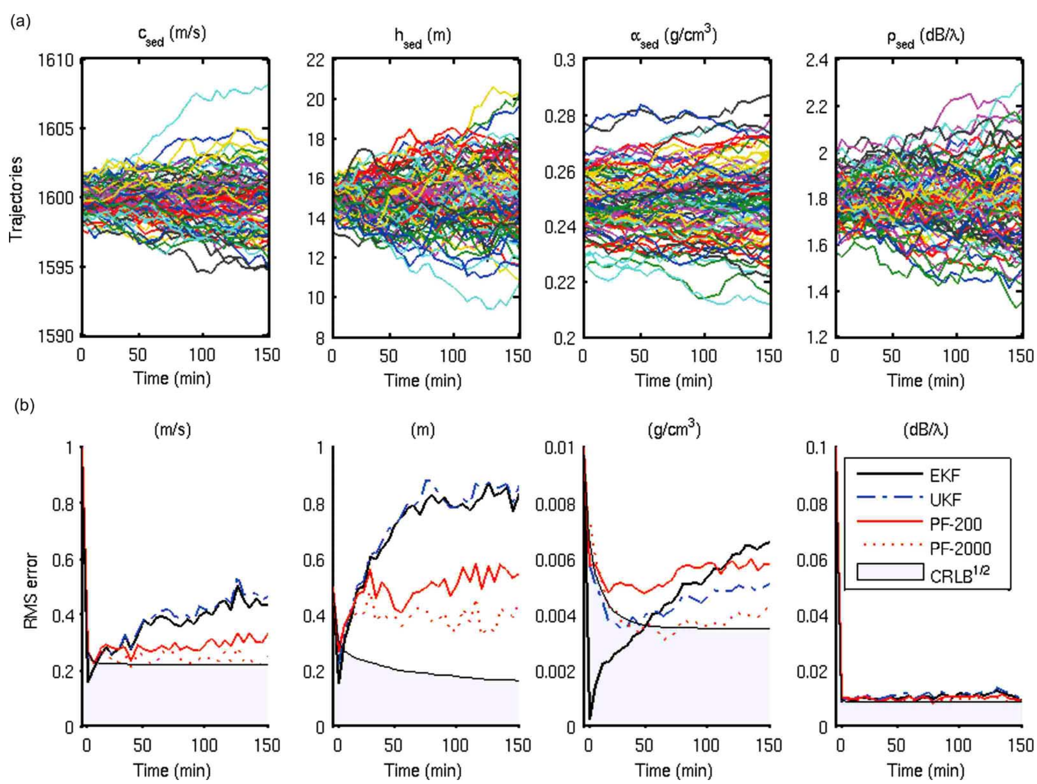

FIG. 3. (Color online) Example 1: Comparison of the tracking algorithms: (a) Evolution of 100 different environments (Monte Carlo trajectories), and (b) RMS errors for the EKF, UKF, 200-point PF, and 2000-point PF obtained from tracking each of these 100 trajectories along with the theoretical lower limit for the RMS error, the square root of the posterior CRLB.

TABLE II. Performance comparison for example 1.

Method	RMS at t=150 min c_{sed} (m/s)	h_{sed} (m)	α_{sed} (dB/λ)	ρ_{sed} (g/cm^3)	Avg. η (%)	RTAMS (100–150 min) c_{sed} (m/s)	h_{sed} (m)	α_{sed} (dB/λ)	ρ_{sed} (g/cm^3)	Avg. % Improv. over EKF
EKF	0.43	0.77	6.5×10^{-3}	10.7×10^{-3}	52	0.44	0.82	6.1×10^{-3}	11.3×10^{-3}	0
UKF	0.45	0.80	5.0×10^{-3}	11.1×10^{-3}	55	0.46	0.84	4.9×10^{-3}	11.8×10^{-3}	2
PF-200	0.30	0.53	5.8×10^{-3}	9.9×10^{-3}	63	0.31	0.54	5.8×10^{-3}	10.4×10^{-3}	19
PF-2000	0.22	0.39	4.2×10^{-3}	9.3×10^{-3}	80	0.24	0.39	3.9×10^{-3}	9.6×10^{-3}	36
PF-10 000	0.22	0.39	4.2×10^{-3}	9.3×10^{-3}	81	0.24	0.39	3.9×10^{-3}	9.6×10^{-3}	37
$\sqrt{\text{PCRLB}}$	0.22	0.16	3.5×10^{-3}	8.8×10^{-3}	100	0.22	0.17	3.5×10^{-3}	8.8×10^{-3}	48

previous classical geoacoustic inversion techniques. The forward model runs are by far the most computationally intensive section in a geoacoustic inversion or tracking problem. Therefore, the computational costs are given in terms of the number of forward models needed to run at each step k. First, if these parameters were to be inverted as a geoacoustic inversion problem using a global optimizer such as genetic algorithms, one would need around 10 000–40 000 forward model runs[1,8] for each step k. If the uncertainties or the parameter PDF are also required, techniques such as importance,[10] Gibbs,[4] and Metropolis–Hastings sampling[11,12,33] would be needed at each step requiring typically 100 000–1 000 000 samples per k. Using a hybrid genetic algorithms–Markov chain Monte Carlo (GA-MCMC) sampler may reduce this number,[34] but still the required number of forward model runs is large compared to the techniques discussed here. Instead, geoacoustic tracking requires an initial mean and a PDF that is obtained by running a classical geoacoustic inversion at $k=0$ and then tracking this density, and the optimum solution is done using the filter. The EKF requires $2\times n_x$ forward model runs at each step to compute the Jacobians needed for linearization and one forward model at the prediction step (nine forward model runs per k for this particular example). Similarly, the UKF uses $(2\times n_x+1)$ sigma points to propagate the mean and covariance using the unscented transformation (UT). The PF-200, −2000, and −10 000 require factors of 20, 200, and 1000 more CPU time than those of the EKF, respectively, for this scenario. Therefore, the selection of the filter type is a trade-off between the gain in performance and the extra computational burden of the PF.

Since the PF is computationally expensive compared to the KFs, it is desirable to know how much improvement can be obtained by using PF with a large number of particles. Unfortunately, the optimum n_p is scenario dependent. The effect of increasing particle size for this problem is shown in Fig. 4. A value of around 2000 particles per k provides maximum filter efficiency (81%) with minimum computational cost.

B. Example 2: Divergence analysis for slowly and fast changing environments

Divergence is an important issue in tracking problems. There are many reasons a track will diverge, such as the limitations in the filter (e.g., a KF structure in a highly non-Gaussian problem), errors in the forward model, and incorrect assumptions about the state and/or measurement noise. A frequently encountered problem is the error in the state equation model. The state equation models how we expect the state parameters to behave with k. If the real values of the state parameters evolve differently from this state evolution model, the filter may be unable to track these changes. Even though the measurement equation may tell the filter that the parameters are changing in an unexpected way, the filter may ignore the measurement information coming from Eq. (3) if this contradicts the state evolution model in Eq. (2). The filter type selected will affect the level of state modeling error that can be handled without resulting in divergence.

Geoacoustic tracking is no different. The state model used here assumes that the environment is evolving slowly. Therefore, comparing filter behavior under both slowly and fast changing environments is desirable. The environment in Fig. 2 is selected with n_x=7 environmental parameters to track, with the same VLA configuration and forward model as in the previous example. The simulation and measurement configuration parameters are selected from the sensitivity

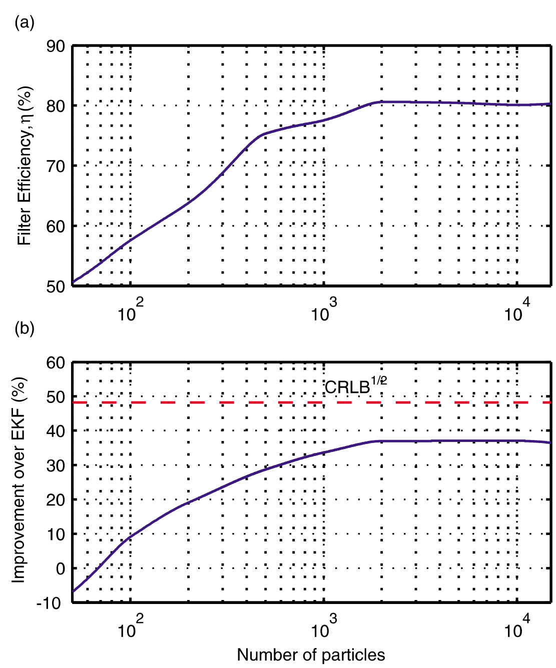

FIG. 4. (Color online) Example 1: Performance improvement of PF as a function of number of particles expressed in terms of (a) filter efficiency, and (b) improvement over the EKF. The dashed line shows the attainable improvement limit.

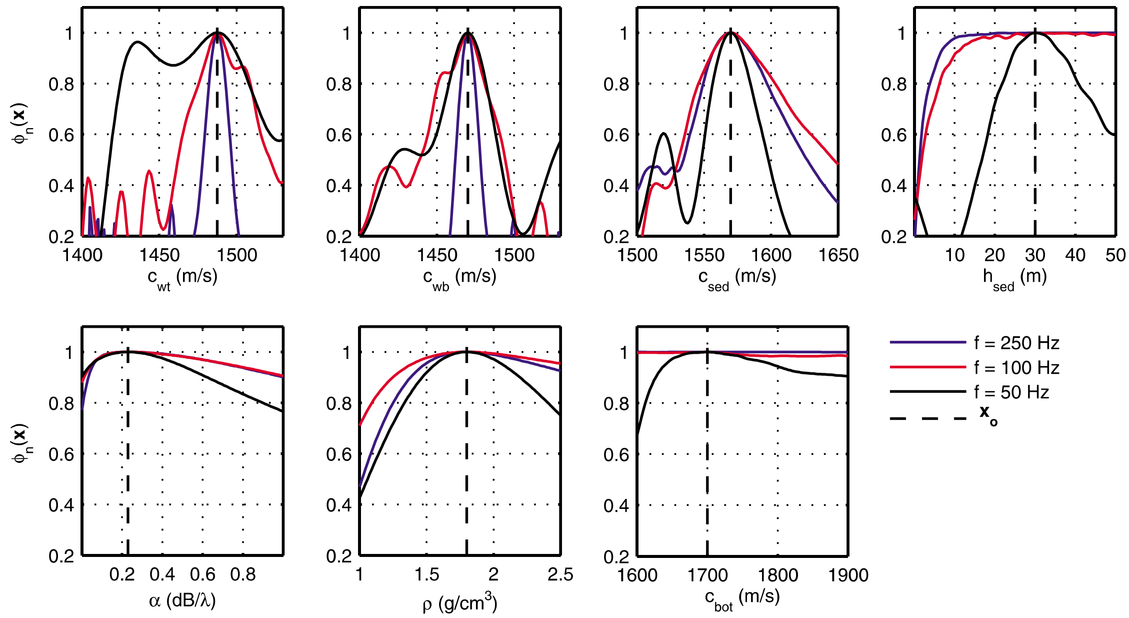

FIG. 5. (Color online) Example 2: Normalized objective functions for three different frequencies. The cost function for each parameter is obtained by fixing all other parameters to their true values (dashed line).

plots at $t=0$, given in Fig. 5. These plots are obtained by varying one parameter at a time from their values at $t=0$, while the other six are the same as those of $\mathbf{x}_0$. The normalized objective function used here is similar to ones used in Refs. 20 and 10 as a MSE metric. It is given as

$$\Phi_n(\mathbf{x}) = 1 - \frac{1}{\mathbf{y}_k^H \mathbf{y}_k} \left\| \mathbf{y}_k - \frac{\mathbf{d}(\mathbf{x}_k)^H \mathbf{y}_k}{\|\mathbf{d}(\mathbf{x}_k)\|^2} \mathbf{d}(\mathbf{x}_k) \right\|^2. \tag{10}$$

The objective functions in Fig. 5 are given for three different frequencies at 50, 100, and 250 Hz, respectively. Note that the penetration depth of the field decreases as the frequency is increased. Since the source and VLA are separated by 5 km, most of the high-incidence angle deep penetrating modes have attenuated at longer ranges and may not be detected by the receiver array. Note that $\Phi_n(\mathbf{x})$ for sediment thickness becomes insensitive after a certain value, which decreases with increasing frequency. The same also applies to the bottom sound speed. For the given environment, most of the signal is restricted to the sediment, not penetrating deep enough; hence $\Phi_n(\mathbf{x})$ is not sensitive to the bottom parameters.

Simulation parameters different from the previous example are provided in Table III. The tracking is carried out for 200 min with one update every 2 min. A frequency of 250 Hz is selected for the tracking problem. At this frequency, the bottom parameters give an entirely flat sensitivity plot, and sediment thickness above around 20 m is poorly determined. The evolutions of the seven parameters are given as solid lines in Fig. 6. These variations include a fluctuation in the top water sound speed, simultaneous gradual variations in all seven parameters, and a simultaneous sudden jump in two sediment parameters, sediment thickness from 30 to 20 m followed by a similar increase in the sediment sound speed. Note that one of the two environmental parameter jumps is in the sediment, a poorly determined parameter. Therefore, the filters are expected to give high divergence percentages due to the selection of such an environment and frequency, enabling a comparison between them under conditions difficult for tracking purposes. The evolving environment is tracked using the EKF, UKF, and PF that use 200, 2000, and 5000 particles, respectively. PF-2000 results are not shown in Fig. 6 but are given in Table IV.

The corresponding temporal evolution of the amplitude of the vertical acoustic field at 5 km as a function of time is given in Fig. 7. Note how the vertical mode structure evolves with time. Also note that only a sampled version of this field is used in tracking, as shown in the figure as circles representing the vertical hydrophone locations of the VLA. A lower spatial sampling frequency of the vertical field may result in the loss of some of the evolving trends in the field and higher divergence rates.

A typical track result for each filter is given in Fig. 6 along with the true trajectories of the parameters, and the results are summarized in Table IV. Some of the important

TABLE III. Simulation parameters for example 2.

Parameter	c_{wt} (m/s)	c_{wb} (m/s)	c_{sed} (m/s)	h_{sed} (m)	α (dB/λ)	ρ (g/cm^3)	c_{bot} (m/s)
State noise $\mathbf{Q}_k^{1/2}$	0.5	0.5	0.5	1.0	0.002	0.02	1.5
Initial cov. $\mathbf{P}_0^{1/2}$	1.0	1.0	1.0	1.0	0.002	0.02	3.0
Divergence threshold	1.0	1.0	1.0	1.0	0.01	0.05	10.0

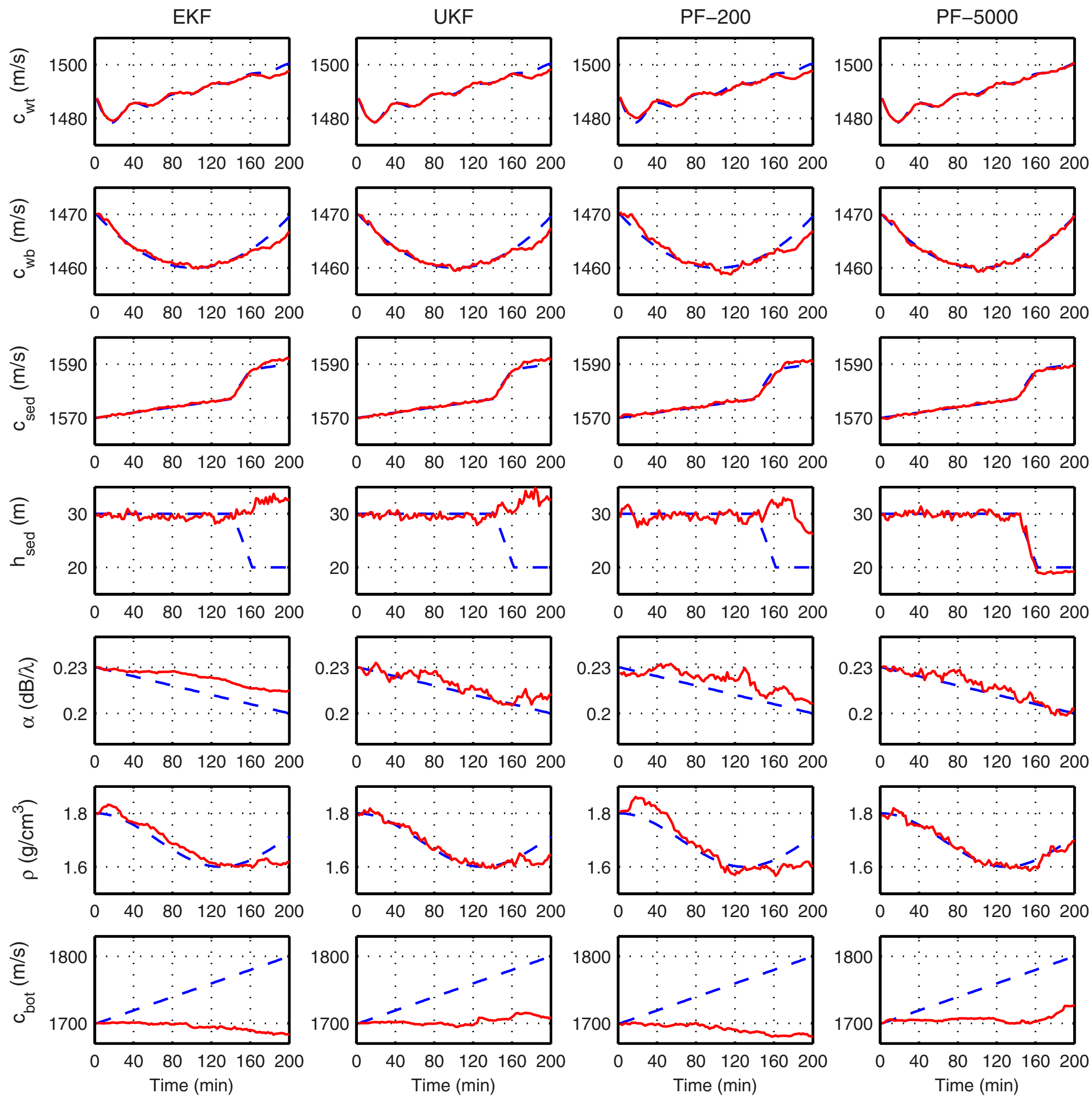

FIG. 6. (Color online) Example 2: Tracking results of EKF, UKF, PF-200, and PF-5000 for the seven-parameter environment given in Fig. 1 using the long range VLA. True trajectories (dashed) are provided along with the tracking filter estimates (solid).

features in this figure are as follows:

- All four filters are sensitive to the water column sound speed parameters and are able to track them. Water column parameters only start to diverge after the jump at $t = 140$ min for the EKF, UKF, and PF-200 because these filters are unable to track some of the sediment parameters that are coupled to the water column sound speed values. The PF-5000 is able to track these parameters perfectly both during slow ($t < 140$ min) and rapid ($t >= 140$ min) changes. Although the PF-200 could track the slowly changing sound speed values, the track is much noisier than the KF filters and the high-particle PF. A similar pattern emerges for the sediment density.
- All four filters are mostly able to track the sediment sound

TABLE IV. Results for example 2.

	After 140 min			After 200 min					
						% divergence			
Method	RTAMS h_{sed} (m)	% Imp. EKF	% Avg. Diverg.	RTAMS h_{sed} (m)	% Imp. EKF	$c_{w,sed}$	h_{sed}	α	ρ
EKF	0.75	0	16	10.6	0	82	100	68	6
UKF	0.71	24	0	11.2	15	62	100	1	12
PF-200	2.92	−70	39	9.2	3	58	90	61	48
PF-2000	0.83	16	1	4.8	42	29	40	7	12
PF-5000	0.82	20	0	3.1	60	11	19	1	5

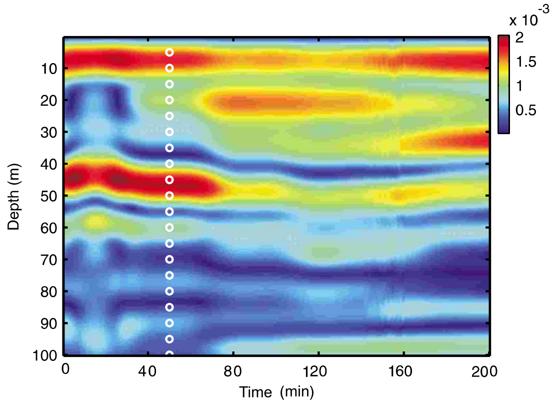

FIG. 7. (Color online) Example 2: Evolution of the magnitude of the vertical acoustic field in the water column at the receiver array as the environment evolves in time. Hydrophone locations (circle) show the vertical sampling interval of the time-varying field.

speed, including the sudden jump in the parameter. Again, the track given by PF-5000 is superior to the other three.

- As expected, the first three filters fail to track the sudden jump in the sediment thickness. Only PF-5000 is able to track the true trajectory. Also note how noisy the track is even for the PF-5000 due to the low sensitivity predicted in Fig. 5.
- Attenuation is the only parameter where there is a marked difference between the EKF and the UKF. The improvements introduced by the UKF over the linearized EKF enable it to track the attenuation, whereas the EKF divergence rates are much higher. PF-200 performance lies somewhere between the two KFs, and PF-5000 performance is very similar to the UKF performance, except for the superior performance after the jump due to divergence of other parameters in the UKF.
- All four filters are unable to track the bottom sound speed. This is an expected result, taking into account the entirely flat sensitivity curve given in Fig. 5.

The divergence percentages are given in Table IV for slowly changing (before $t=140$ min) and fast changing (after $t=140$ min) environments. A parameter track is declared diverged if the RMS error is greater than the corresponding threshold given in Table III for any 30 consecutive min (i.e., 15 samples). All the average values in Table IV are computed using the first six parameters, excluding the bottom sound speed, which always diverge. Note how the KFs have low RTAMS for the sediment thickness compared to the RTAMS of PFs before the jump. The average improvement over EKF is 20% for PF-5000, and overall, the UKF performs best in this region. The UKF, PF-2000, and PF-5000 almost always successfully track the trajectory, while the average divergence rates are 16% and 39% for the EKF and PF-200, respectively.

However, both KFs have difficulties at the jump in the sediment thickness. The UKF still outperforms the EKF by 15%, but the improvement goes up to 60% for the PF-5000 (Table IV). The average divergence in the water column and sediment layer sound speed values (designated as $c_{w,\text{sed}}$) are given after the jump. The UKF diverges less than the EKF in sound speed tracking and more in attenuation tracking, both filters have a 100% divergence for the sediment thickness, and the UKF still tracks the attenuation whereas the EKF diverges 68% of the time after the jump. The PF-5000, on the other hand, diverges only 19% of the time for the hard-to-track sediment thickness, and overall, the PF performs much better than the KF structures after the jump.

It is also of interest to observe the underlying PDFs of the evolving parameters and examine how the uncertainty in parameters change with filter. The evolving PPD of the sediment thickness as a function of time is given for a PF-10 000 and the EKF in Fig. 8. They start with the same initial Gaussian PDF as seen at $t=0$. Both filters are able to follow the parameter until the sudden decrease in the sediment thickness. Note that the PDF of the EKF is always a Gaussian (due to the initial Gaussian assumption and linearization), whereas the PF density can take different forms, which enables the filter to simultaneously follow multiple regions in the state space with high likelihoods (such as at $t=116$ and 152 min. As the parameter starts to evolve quickly, the EKF is unable to follow, and it diverges, as can be seen from the large error in the PDFs given after $t=140$ min between the PF and the EKF. Note how stable the PDF evolution in Fig. 8(b) is at $h_{\text{sed}}=20$ m compared to the 30 m sediment thickness region due to the flat sensitivity curve for larger sediment thickness values.

C. Example 3: Spatial tracking using a HLA

The final example uses a HLA towed together with the source to map the spatially evolving environment. The configuration in Fig. 1(b) is used with a HLA of 254 m and a distance of 300 m from the source.[1] A nonoverlapping spatial partitioning with each step k representing 500 m is selected. Since the source and HLA are close to each other, the complex normal mode code ORCA capable of computing the near field is used as the forward model. The simulation parameters different from the previous examples are summarized in Table V. Again the seven-parameter environment in Fig. 2 is used. To compare the effects of different configurations on an identical geoacoustic tracking problem, the evolution of the environmental parameters is the same as in the previous example.

A typical track for each type of filter is shown in Fig. 9. Note how the tracking capabilities of the filters for individual parameters change from the previous long-range VLA configuration to the short-range HLA configuration used here. Geoacoustic tracking behaves very similarly to previous studies comparing geoacoustic inversions using HLA versus VLA in that a parameter that is not readily estimated by geoacoustic inversion will also be poorly tracked.[1,5,35] The major difference of a source close to the receiver is the ability of the receiver to detect higher order modes with large incidence angles that can penetrate deeper into the sediment since the signal does not propagate enough to attenuate these fields. This means that the field across the HLA is much more sensitive to some of the sediment and bottom parameters such as the bottom sound speed and sediment thickness. Notice how all four filters are able to track, in general, the

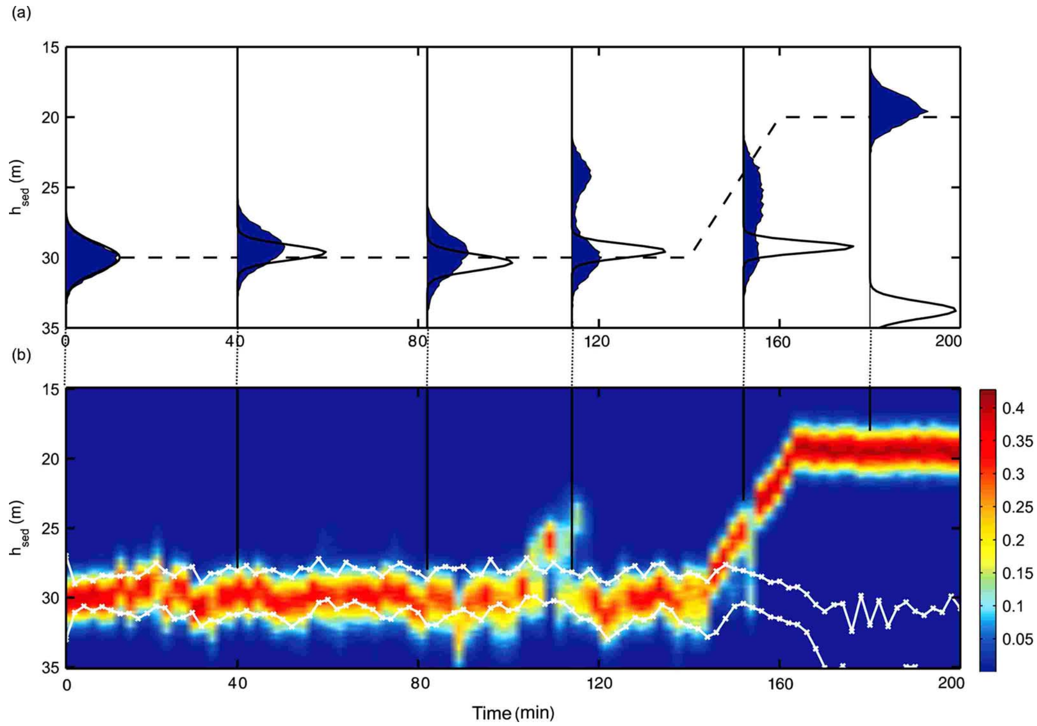

FIG. 8. (Color online) Example 2: Posterior probability density evolution $p(\mathbf{x}_{k|k})$ for the sediment thickness h_{sed} for a 10000-point particle filter and the EKF: (a) Six snapshots at $t=0$, 40, 84, 116, 152, and 180 min with the local particle histograms representing the PF distribution (solid) and the EKF Gaussian PDF (line) along with the true trajectory (dashed). (b) The continuous evolution of the PF PPD together with the local mean ± 3 standard deviation $(\hat{\mathbf{x}}_{k|k} \pm 3\sqrt{\mathbf{P}_{k|k}})$ of the EKF Gaussian.

bottom sound speed, sediment thickness, sediment sound speed, and density both in slowly and fast changing environments. Since the field is not that sensitive to the attenuation, it is now a relatively poorly determined parameter and the EKF fails to track it, while the UKF and PF-5000 are able to maintain the track, albeit a noisy one. Similarly, the filters are unable to track the top sound speed value most of the time. Only PF is able to track this parameter on occasion.

The improvement percentages of the filters are obtained by repeating the track using 100 MC realizations. The results are given in Table V. The improvement of the UKF over EKF is similar to the previous example with 25% and 33% for slowly and fast changing regions, respectively. PF-200 performs poorly due to an insufficient number of particles used in tracking. On the other hand, the PF-5000 outperforms the EKF by 60%.

V. DISCUSSION

It is possible to extend the state space from just the environmental parameters by appending other parameters-of-interest such as the source range, depth, and speed. Also a single frequency is used throughout the paper. However, multiple frequencies are frequently employed for geoacoustic inversion due to the varying levels of sensitivities to different frequencies and robustness. It is possible to include multiple frequencies by appending the array data at different frequencies forming a long measurement vector $\mathbf{y}_k$ and a forward model $\mathbf{h}(\mathbf{x}_k)$ composed of multiple normal mode runs at different frequencies.

The filter performance strongly depends on where $\mathbf{x}$ is in the state space. The most common scenario is where the performance improves from the EKF to the UKF to a PF with enough particles. However, there are regions in the state space where the KFs give better tracking results depending on the local linearity of the forward model and the Gaussian nature of the densities involved.

Although not given here, there are some special cases in geoacoustic tracking that can result in track divergence. One example observed during spatial tracking using the HLA configuration (example 3) is when a layer gets thin and then

TABLE V. Simulation parameters and percent improvement of filters for example 3.

Simulation parameters				Method	% Imp. over EKF 35 km	% Imp. over EKF 50 km
Source depth	20 m	Source frequency	100 Hz			
Receiver type	HLA	Array SNR ($\mathbf{R}_k$)	40 dB	EKF	0	0
Receiver depth	26 m	Array start, Δr	300 m, 2 m	UKF	25	33
No. of hydrophones	128	Track length	50 km (k=100)	PF-200	−12	−73
MC runs	100	Track frequency	1 meas./500 m	PF-5000	60	64

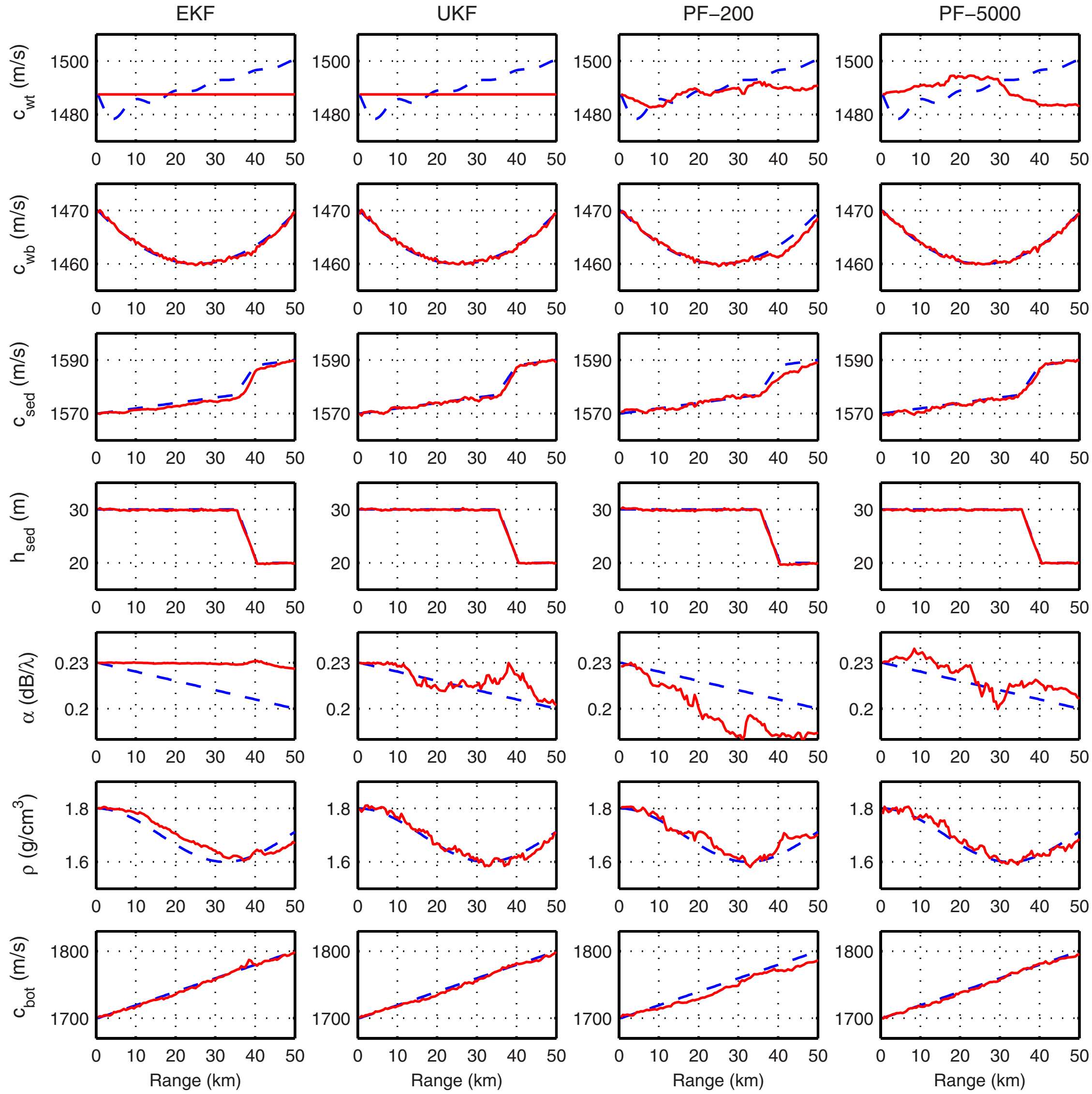

FIG. 9. (Color online) Example 3: Tracking results of EKF, UKF, PF-200, and PF-5000 for the seven-parameter environment given in Fig. 1 using the short range HLA configuration. True trajectories (dashed) are provided along with the tracking filter estimates (solid).

thickens again. When the layer gets thin, other parameters such as the sound speed, attenuation, and density characterizing the layer have little or no effect on the acoustic field across the array, temporarily making the field insensitive to that layer's parameters. This results in deviations from their true values for these parameters, and when the layer starts to thicken again the filters diverge since the starting points for the layer parameters other than the layer thickness are too far from their current true values.

Another case is the coupling between the parameters. When the sediment thickness increases, less signal reaches the bottom layer, resulting in degrading performance of these bottom parameters similar to the previous case and may cause divergence as the sediment gets less thick again. In general, PFs show more robust tracking under such conditions.

Also the seabed can have spatial layer changes. While one sediment layer and a semi-infinite bottom are adequate initially, a second sediment layer can form. Or the sediment type becomes sand, whereas the model given to the PF assumed that the region is clay, limiting the possible parameter values via priors. Such environments can be tracked using multiple environmental models, one for each possible scenario. This will require Gaussian sum filters such as the interactive multiple model EKF/UKF that involves a filter bank composed of multiple KFs running in parallel for each possible model.[29,36] Similarly, this can be accomplished using their PF counterpart, the MMPF.[37]

One interesting observation from the simulations is the KFs ability to continue to track some parameters while other parameters diverge and can only be tracked by the PF. This means that the marginal densities for these parameters are close to Gaussian and the measurement equations connecting those parameters to the acoustic field are close to being linear. This is unlike many other tracking problems such that when one parameter starts to diverge, so do all the others, usually resulting in a total divergence. However, there are many cases where such marginal Gaussian densities occur. In these cases, one common approach is to use a Rao–Blackwellized particle filter also known as the marginalized particle filter that groups the state parameters into linear/ Gaussian and nonlinear/non-Gaussian ones and uses a mixed EKF/PF approach, reducing the dimension of the state space that the PF has to sample, which, in return, reduces significantly the required number of particles for a desired accuracy.[29,38]

VI. SUMMARY

Tracking of geoacoustic environmental parameters has been addressed. Spatial and temporal evolutions of the water column and seabed parameters were estimated using EKFs, UKFs, and PFs with acoustic measurements as inputs. These tracking filters enabled providing real-time, continuously updated estimates of the geoacoustic parameters and their uncertainties, requiring far fewer forward model runs compared to alternatives such as successively running geoacoustic inversion algorithms.

This paper investigated how the three filters behaved for the nonlinear, non-Gaussian geoacoustic tracking problem using three examples with both the VLA and HLA simulated data. An efficient way of computing the local PCRLB to compute the filter efficiencies was shown. The results showed that all three filters performed well in geoacoustic applications. It was found that a PF with enough particles could typically achieve 80% filter efficiency in geoacoustic tracking while providing PPD evolutions for the environmental parameters. Even though KFs had less efficiency and high divergence rates and were unable to track some parameters while the PF was still able to maintain track, they also showed robust tracking in many cases. Since they are computationally very fast compared to the PF, they can be used in many applications where the performances are similar. The UKF outperformed the EKF in most of the simulations, but the improvement-over-EKF values of the UKF were modest compared to the PF. The PF was able to maintain track in environments that include sudden changes such as the sediment thickness. The two KFs used here showed mixed success in tracking sudden jumps in the parameter values.

PFs proved to be very promising in the nonlinear, non-Gaussian geoacoustic tracking problem. It was shown that the performance could degrade below that of the EKF if a small number of particles were used. However, in this paper, the PF with enough particles showed robust tracking in a number of cases involving different measurement configurations that use HLA and VLA data, slowly and quickly changing environments, and environmental parameters with relatively flat sensitivity curves. The limitations of all three filters were discussed using an example of tracking a quickly changing environment with parameters having medium to totally flat sensitivity curves.

ACKNOWLEDGMENT

This work was supported by the Office of Naval Research under Grant No. N00014-05-1-0264.

APPENDIX A: FILTER EQUATIONS

1. Extended Kalman filter

The first filter choice is the EKF (Ref. 22). Since KF is the best possible linear tracking filter, its extended version that can operate on nonlinear systems can still be near optimal. The EKF works by converting the system into a form over which the KF can operate. This is done by locally linearizing the equations using the first terms in the Taylor series expansions of the nonlinear transformations (such as the normal mode code in $\mathbf{h}$) and assuming that the nonlinearities are small so that EKF will perform well. Once the equations are linearized, starting with a Gaussian PDF for $\mathbf{x}_0$ will ensure that the evolving parameters will remain Gaussian, and it is necessary to propagate only the mean and covariance as in the KF. However, due to this approximation, the EKF cannot claim the optimality enjoyed by the KF for linear-Gaussian systems. The EKF has been implemented successfully in a large number of applications such as radar and sonar target tracking applications, and its speed and ease of implementation make the EKF the filter of choice.

In geoacoustic tracking, the complex source magnitude s_k is usually not known. Therefore, the EKF equations are modified by inserting a maximum likelihood (ML) estimator that estimates the source every time the forward normal $\mathbf{d}(\mathbf{x}_k)$ is run.[10] This is done by writing the likelihood function at step k as

$$\mathcal{L}(\mathbf{x}_k) = \frac{1}{\pi^{n_H}|\mathbf{R}|} \exp[-(\mathbf{y}_k - s_k\mathbf{d}(\mathbf{x}_k))^H \mathbf{R}^{-1}(\mathbf{y}_k - s_k\mathbf{d}(\mathbf{x}_k))], \tag{A1}$$

where n_H is the number of hydrophones. Assuming that the complex Gaussian noise $\mathbf{w}_k$ is uncorrelated with the same variance along the array ($\mathbf{R}=\nu\mathbf{I}$),

$$\mathcal{L}(\mathbf{x}_k) = \frac{1}{(\pi\nu)^{n_H}} \exp\left(-\frac{\|\mathbf{y}_k - s_k\mathbf{d}(\mathbf{x}_k)\|^2}{\nu}\right). \tag{A2}$$

The ML estimate for the source s_k is then obtained by solving for $\partial\mathcal{L}/\partial s_k=0$, giving

$$\hat{\mathbf{s}}_k = \frac{\mathbf{d}(\mathbf{x}_k)^H\mathbf{y}_k}{\|\mathbf{d}(\mathbf{x}_k)\|^2}. \tag{A3}$$

This source estimate is used in the following EKF equations both for the calculation of $\mathbf{h}$ and during the linearization of $\mathbf{h}$ to obtain the matrix $\mathbf{H}$:

$$\hat{\mathbf{x}}_{k|k-1} = \mathbf{F}\hat{\mathbf{x}}_{k-1|k-1}, \tag{A4}$$

$$\mathbf{P}_{k|k-1} = \mathbf{Q}_{k-1} + \mathbf{F}\mathbf{P}_{k-1|k-1}\mathbf{F}^T, \tag{A5}$$

$$\hat{\mathbf{x}}_{k|k} = \hat{\mathbf{x}}_{k|k-1} + \mathbf{K}_k(\mathbf{y}_k - \mathbf{h}(\hat{\mathbf{x}}_{k|k-1})), \tag{A6}$$

$$\mathbf{P}_{k|k} = \mathbf{P}_{k|k-1} - \mathbf{K}_k\mathbf{S}_k\mathbf{K}_k^T, \tag{A7}$$

where

$$\mathbf{S}_k = \hat{\mathbf{H}}_k\mathbf{P}_{k|k-1}\hat{\mathbf{H}}_k^T + \mathbf{R}_k, \tag{A8}$$

$$\mathbf{K}_k = \mathbf{P}_{k|k-1}\hat{\mathbf{H}}_k^T\mathbf{S}_k^{-1}, \tag{A9}$$

$$\mathbf{h}(\hat{\mathbf{x}}_{k|k-1}) = \frac{\mathbf{d}(\hat{\mathbf{x}}_{k|k-1})^H \mathbf{y}_k \mathbf{d}(\hat{\mathbf{x}}_{k|k-1})}{\|\mathbf{d}(\hat{\mathbf{x}}_{k|k-1})\|^2}, \tag{A10}$$

$$\hat{\mathbf{H}}_k = [\nabla_{\mathbf{x}_k} \mathbf{h}^T(\hat{\mathbf{x}}_{k|k-1})]^T. \tag{A11}$$

Equations (A4) and (A5) are the prediction steps that give the environmental model estimate $\hat{\mathbf{x}}_k$ and its associated uncertainty in terms of the covariance matrix $\mathbf{P}_k$ at step index k given the previous history $\{\mathbf{x}_0, \mathbf{x}_1, \ldots, \mathbf{x}_{k-1}\}$, Eqs. (A6) and (A7) are the correction equations that give $\hat{\mathbf{x}}_k$ and $\mathbf{P}_k$ at step index k given its previous history $\{\mathbf{x}_0, \mathbf{x}_1, \ldots, \mathbf{x}_{k-1}\}$ and the set of measurements $\{\mathbf{y}_1, \mathbf{y}_2, \ldots, \mathbf{y}_k\}$, and $\mathbf{K}$ is the Kalman gain.

Note that the insertion of the ML estimate of the source in Eq. (A3) into the Kalman update equation violates the Kalman formulation. This is true for Eq. (A6) where the Kalman gain is applied to the measured minus predicted data $(\mathbf{y}_k - \mathbf{y}_{\text{pred}})$ since the predicted data include $\mathbf{y}_k$ itself due to the ML source estimate in Eq. (A3). However, the ML estimator in Eq. (A3) simply normalizes the amplitude of the predicted data so that the acoustic field variation across the array is compared, not the actual amplitudes, eliminating the effects of the unknown source amplitude. Moreover, the averaging inherent in the inner product in Eq. (A3) over the array elements makes the source estimate less noisy and more robust relative to the environmental parameters. Finally, the performance calculations of the KFs used here are not affected since the synthetic data enable us to compute the true filter RMS error $E[(\hat{\mathbf{x}}_{k|k} - \mathbf{x}_{k|k})^2]$ instead of the conventional performance metric for the KF (covariance matrix $\mathbf{P}_{k|k}$). An alternative approach would be to include the unknown source term into the state model $\mathbf{x}_k$. However, this will increase the dimension of the state space for a nuisance parameter in which we are not interested.

2. Unscented Kalman filter

The analytical linearization used in the EKF results in poor estimates of the mean and covariance as the nonlinearity in the forward model increases. To mitigate this the UKF[23,39] has been introduced. Instead of analytical linearization, the UKF uses a concept called statistical linearization in which the filter enforces Gaussianity and keeps the nonlinearity. Enforcing Gaussian PDFs enables the filter to carry all the necessary information by propagating only the mean and covariance as does the KF. This is achieved by the UT that enables the propagation of the mean and variance through nonlinear functions. The UKF represents initial densities using only a few predetermined particles called sigma points. These points are chosen deterministically by the UT algorithm, and they describe accurately the mean and covariance of a PDF. As the random variable undergoes a nonlinear transformation, these points are propagated through the nonlinear function and used to reconstruct the new mean and covariance using the UT weights. Hence, unlike the EKF, they can compute accurately the mean and covariance to at least second order (third if the initial PDF is Gaussian) of the nonlinearity.

Similar to the EKF, the UKF algorithm used here incorporates a ML estimator for the unknown source term. The UKF uses the following recursive formulation where $2n_x+1$ sigma points $\{\mathcal{X}^i\}_{i=0}^{2n_x}$ and their corresponding weights W^i are generated and used with the UT algorithm to perform the mean $(\hat{\mathbf{x}}_k)$ and covariance $(\mathbf{P}_k)$ calculations required in the Kalman framework. The UT weights are given in terms of the scaling parameter $\lambda = \alpha^2(n_x+\kappa) - n_x$ and prior knowledge parameter β, where α is used to control the spread of the sigma points around the mean and κ is the secondary scaling parameter. α, β, and κ are taken as 0.1, 2, and 0, respectively.

UT weights and sigma points are generated using

$$\mathcal{X}_{k-1}^0 = \hat{\mathbf{x}}_{k-1|k-1},$$

$$W_m^0 = \frac{\lambda}{n_x + \lambda}, \quad W_{\text{cov}}^0 = W_m^0 + \beta + 1 - \alpha^2, \tag{A12}$$

$$\mathcal{X}_{k-1}^i = \hat{\mathbf{x}}_{k-1|k-1} \pm \left(\sqrt{(n_x + \kappa)\mathbf{P}_{k-1|k-1}}\right)_i,$$

$$W_m^i = W_{\text{cov}}^i = \frac{0.5}{n_x + \lambda}, \quad i = 1, 2, \ldots, 2n_x, \tag{A13}$$

where $(\sqrt{.})_i$ is the ith column of the matrix square root. The prediction step is composed of

$$\mathcal{X}_{k|k-1}^i = \mathbf{F}\mathcal{X}_{k-1}^i, \quad \mathcal{Y}_{k|k-1}^i = \frac{\mathbf{d}(\mathcal{X}_{k|k-1}^i)^H \mathbf{y}_k \mathbf{d}(\mathcal{X}_{k|k-1}^i)}{\|\mathbf{d}(\mathcal{X}_{k|k-1}^i)\|^2},$$

$$\hat{\mathbf{x}}_{k|k-1} = \sum_{i=0}^{2n_x} W_m^i \mathcal{X}_{k|k-1}^i, \quad \hat{\mathbf{y}}_{k|k-1} = \sum_{i=0}^{2n_x} W_m^i \mathcal{Y}_{k|k-1}^i,$$

$$\mathbf{P}_{k|k-1} = \mathbf{Q}_{k-1} + \sum_{i=0}^{2n_x} W_{\text{cov}}^i [\mathcal{X}_{k|k-1}^i - \hat{\mathbf{x}}_{k|k-1}][\mathcal{X}_{k|k-1}^i - \hat{\mathbf{x}}_{k|k-1}]^T, \tag{A14}$$

and the update step uses

$$\mathbf{P}_{xy} = \sum_{i=0}^{2n_x} W_{\text{cov}}^i [\mathcal{X}_{k|k-1}^i - \hat{\mathbf{x}}_{k|k-1}][\mathcal{Y}_{k|k-1}^i - \hat{\mathbf{y}}_{k|k-1}]^T,$$

$$\mathbf{P}_{yy} = \sum_{i=0}^{2n_x} W_{\text{cov}}^i [\mathcal{Y}_{k|k-1}^i - \hat{\mathbf{y}}_{k|k-1}][\mathcal{Y}_{k|k-1}^i - \hat{\mathbf{y}}_{k|k-1}]^T,$$

$$\mathbf{K}_k = \mathbf{P}_{xy}(\mathbf{P}_{yy} + \mathbf{R}_k)^{-1}, \tag{A15}$$

$$\hat{\mathbf{x}}_{k|k} = \hat{\mathbf{x}}_{k|k-1} + \mathbf{K}_k(\mathbf{y}_k - \hat{\mathbf{y}}_{k|k-1}), \tag{A16}$$

$$\mathbf{P}_{k|k} = \mathbf{P}_{k|k-1} - \mathbf{K}_k(\mathbf{P}_{yy} + \mathbf{R}_k)\mathbf{K}_k^T. \tag{A17}$$

Although it is fast relative to more advanced techniques, derivative-free, and an improvement over the EKF, there still are two weaknesses. The first is that the nonlinearity may be so severe that it may require an even higher order accuracy than the UKF can provide to correctly capture the mean and covariance. The other is that the densities may be highly non-Gaussian so that the first two moments will not be sufficient even if they can be calculated correctly.

3. Particle filter

The third algorithm used in this paper is the SMC commonly known as the PF.[24] Rapid increases in the available computational power have made the PF very popular for many nonlinear, non-Gaussian tracking problems. Unlike the Kalman framework, neither Gaussian nor linearity assumptions are necessary for the PF. However, this means that propagating only the mean and covariance is not sufficient anymore. Instead, the PF propagates an ensemble of particles to represent the densities. These particles are selected randomly by MC runs. Compared with the sigma points of the UKF, a much larger number of particles are needed to represent the PDF. Therefore, the PF can perform much better than its KF variants, but it does this with an order of magnitude increase in the required computational resources. There are many different variants[29] of the PF such as the regularized particle filter, Markov chain MC step PF, and auxiliary and classical SIR PFs. The SIR (Ref. 40) algorithm is used throughout this work. Normally, degeneracy can be a problem for the SIR algorithm, especially for low process noise systems. However, due to the environmental uncertainty in the model, $\mathbf{Q}_k$ is selected to be relatively large, thus mostly eliminating the need for more complex PFs with improved sample diversity.

The SIR algorithm uses n_p particles $\{\chi_k^i\}_{i=1}^{n_p}$ to represent the PDF at each step k. The filter has the predict and update sections just as in a KF, but the SIR filter will use these sections to propagate the particles instead of mean and covariance calculations. The initial set of particles $\{\chi_0^i\}_{i=1}^{n_p}$ are sampled from the prior $p(\mathbf{x}_0)$. The SIR filter uses the importance sampling[41] density as the transitional prior $p(\mathbf{x}_k|\mathbf{x}_{k-1})$. Although this is a suboptimal choice, it is easy to sample from this density. This selection results in particle weights proportional to the likelihood $W_k \propto p(\mathbf{y}_k|\mathbf{x}_k)$.

The prediction step consists of sampling from the prior. Then the normalized weight W_k^i of each particle is calculated from its likelihood function. As with the KFs, the source term is estimated with a ML estimator during the likelihood calculation of each particle in the ensemble. The update step includes the resampling section where a new set of n_p particles is generated from the parent set according to the weights of the parent particles, with high likelihood particles generating more particles than the low likelihood ones. Hence, a single iteration of the recursive SIR algorithm can be summarized as

$$\{\mathcal{X}_{k|k-1}^i\}_{i=1}^{n_p} \sim p(\mathbf{x}_k|\mathbf{x}_{k-1}), \tag{A18}$$

$$W_k^i = \frac{p(\mathbf{y}_k|\mathcal{X}_{k|k-1}^i)}{\sum_{i=1}^{n_p} p(\mathbf{y}_k|\mathcal{X}_{k|k-1}^i)}, \tag{A19}$$

$$\{\mathcal{X}_{k|k}^i\}_{i=1}^{n_p} = \text{Resample}[W_k^j, \{\mathcal{X}_{k|k-1}^j\}_{j=1}^{n_p}],$$

$$\text{such that } \Pr\{\mathcal{X}_{k|k}^i = \mathcal{X}_{k|k-1}^j\} = W_k^j \tag{A20}$$

APPENDIX B: POSTERIOR CRAMÉR–RAO LOWER BOUND

One issue with the tracking problems is that the computation of the full PCRLB is not feasible. Unlike geoacoustic inversion where there is a fixed number (n_x) of random variables in the model vector $\mathbf{x}$, geoacoustic tracking introduces n_x new random variables with every new step k. Therefore, we will use a $(n_x \times n_x)$ matrix PCRLB$_k$ instead of the full PCRLB matrix. PCRLB$_k$ is defined as the inverse of the filtering information matrix $\mathbf{J}_k$ so that the MSE of any filter estimate at tracking step index k will be bounded as

$$E\{(\hat{\mathbf{x}}_{k|k} - \mathbf{x}_k)(\hat{\mathbf{x}}_{k|k} - \mathbf{x}_k)^T\} \geqslant \mathbf{J}_k^{-1}. \tag{B1}$$

A computationally efficient way of computing this PCRLB recursively for discrete-time nonlinear filtering problems is given in Ref. 42,

$$\mathbf{J}_k = \mathbf{D}_{k-1}^{22} - [\mathbf{D}_{k-1}^{12}]^T(\mathbf{J}_{k-1} + \mathbf{D}_{k-1}^{11})^{-1}\mathbf{D}_{k-1}^{12}, \tag{B2}$$

where

$$\mathbf{D}_{k-1}^{11} = -\mathbf{E}\{\nabla_{\mathbf{x}_{k-1}}[\nabla_{\mathbf{x}_{k-1}} \log p(\mathbf{x}_k|\mathbf{x}_{k-1})]^T\}, \tag{B3}$$

$$\mathbf{D}_{k-1}^{12} = -E\{\nabla_{\mathbf{x}_k}[\nabla_{\mathbf{x}_{k-1}} \log p(\mathbf{x}_k|\mathbf{x}_{k-1})]^T\}, \tag{B4}$$

$$\begin{aligned}\mathbf{D}_{k-1}^{22} = &-E\{\nabla_{\mathbf{x}_k}[\nabla_{\mathbf{x}_k} \log p(\mathbf{x}_k|\mathbf{x}_{k-1})]^T\} \\ &-E\{\nabla_{\mathbf{x}_k}[\nabla_{\mathbf{x}_k} \log p(\mathbf{y}_k|\mathbf{x}_k)]^T\}.\end{aligned} \tag{B5}$$

It is important to note that the computations only require $(n_x \times n_x)$ matrices, and the computation cost is independent of the step index k. The geoacoustic tracking problem with the system of equations defined in Eqs. (2) and (3) has a linear state equation, and both of the random noise sequences $\mathbf{v}$ and $\mathbf{w}$ are additive and Gaussian. Therefore, the above equations can be reduced to[43]

$$\mathbf{D}_{k-1}^{11} = \mathbf{F}^T\mathbf{Q}_{k-1}^{-1}\mathbf{F},$$

$$\mathbf{D}_{k-1}^{12} = -\mathbf{F}^T\mathbf{Q}_{k-1}^{-1}, \tag{B6}$$

$$\mathbf{D}_{k-1}^{22} = \mathbf{Q}_{k-1}^{-1} + E\{\mathbf{H}_k^T\mathbf{R}_k^{-1}\mathbf{H}_k\}, \tag{B7}$$

where $\mathbf{H}_k$ is the jacobian of $\mathbf{h}(\mathbf{x})$ computed similar to Eqs. (A10) and (A11) at its true value $\mathbf{x}_k$. Unfortunately the expectation in Eq. (B7) has to be evaluated numerically using a MC analysis. $\mathbf{D}_{k-1}^{22}$ is computed as

$$\mathbf{D}_{k-1}^{22} = \mathbf{Q}_{k-1}^{-1} + \frac{1}{n_{\mathrm{MC}}}\sum_{j=1}^{n_{\mathrm{MC}}} \nabla\,\mathbf{h}(\mathbf{x}_k^j)\mathbf{R}_k^{-1}[\nabla\mathbf{h}(\mathbf{x}_k^j)]^T, \tag{B8}$$

where n_{MC} is the number of MC trajectories, assuming a Gaussian prior PDF with a covariance matrix $\mathbf{P}_0$. The recursion in Eq. (B2) is initiated with

$$\mathbf{J}_0 = -E\{\nabla_{\mathbf{x}_0}[\nabla_{\mathbf{x}_0} \log p(\mathbf{x}_0)]^T\} = \mathbf{P}_0^{-1}. \tag{B9}$$

Once the PCRLB, the inverse of $\mathbf{J}_k$ in Eq. (B2), is computed, the filters can be compared with each other and the CRLB.

[1]M. Siderius, P. L. Nielsen, and P. Gerstoft, "Range-dependent seabed characterization by inversion of acoustic data from a towed receiver array," J. Acoust. Soc. Am. **112**, 1523–1535 (2002).

[2]D. P. Knobles, R. A. Koch, L. A. Thompson, K. C. Focke, and P. E. Eisman, “Broadband sound propagation in shallow water and geoacoustic inversion,” J. Acoust. Soc. Am. **113**, 205–222 (2003).
[3]D. Battle, P. Gerstoft, W. A. Kuperman, W. S. Hodgkiss, and M. Siderius, “Geoacoustic inversion of tow-ship noise via near-field-matched-field processing,” IEEE J. Ocean. Eng. **28**, 454–467 (2003).
[4]D. Battle, P. Gerstoft, W. S. Hodgkiss, W. A. Kuperman, and P. L. Nielsen, “Bayesian model selection applied to self-noise geoacoustic inversion,” J. Acoust. Soc. Am. **116**, 2043–2056 (2004).
[5]M. R. Fallat, P. L. Nielsen, S. E. Dosso, and M. Siderius, “Geoacoustic characterization of a range-dependent ocean environment using towed array data,” IEEE J. Ocean. Eng. **30**, 198–206 (2005).
[6]D. Tollefsen, S. E. Dosso, and M. J. Wilmut, “Matched-field geoacoustic inversion with a horizontal array and low-level source,” J. Acoust. Soc. Am. **120**, 221–230 (2006).
[7]T. C. Yang, K. Yoo, and L. Y. Fialkowski, “Subbottom profiling using a ship towed line array and geoacoustic inversion,” J. Acoust. Soc. Am. **122**, 3338–3352 (2007).
[8]P. Gerstoft, “Inversion of seismoacoustic data using genetic algorithms and *a posteriori* probability distributions,” J. Acoust. Soc. Am. **95**, 770–782 (1994).
[9]M. D. Collins, W. A. Kuperman, and H. Schmidt, “Nonlinear inversion for ocean-bottom properties,” J. Acoust. Soc. Am. **92**, 2770–2783 (1992).
[10]P. Gerstoft and C. F. Mecklenbräuker, “Ocean acoustic inversion with estimation of *a posteriori* probability distributions,” J. Acoust. Soc. Am. **104**, 808–819 (1998).
[11]S. E. Dosso, “Quantifying uncertainty in geoacoustic inversion. I. A fast Gibbs sampler approach,” J. Acoust. Soc. Am. **111**, 129–142 (2002).
[12]C.-F. Huang, P. Gerstoft, and W. S. Hodgkiss, “Validation of statistical estimation of transmission loss in the presence of geoacoustic inversion uncertainty,” J. Acoust. Soc. Am. **120**, 1932–1941 (2006).
[13]J. V. Candy and E. J. Sullivan, “Sound velocity profile estimation: A system theoretic approach,” IEEE J. Ocean. Eng. **18**, 240–252 (1993).
[14]O. Carrière, J.-P. Hermand, J.-C. L. Gac, and M. Rixen, “Full-field tomography and Kalman tracking of the range-dependent sound speed field in a coastal water environment,” J. Mar. Syst. In press (2008).
[15]I. Zorych and Z.-H. Michalopoulou, “Particle filtering for dispersion curve tracking in ocean acoustics,” J. Acoust. Soc. Am. **124**, EL45–EL50 (2008).
[16]A. A. Ganse and R. I. Odom, “Adapting results in filtering theory to inverse theory, to address the statistics of nonlinear geoacoustic inverse problems,” J. Acoust. Soc. Am. **120**, 3357–3357 (2006).
[17]F. B. Jensen and M. C. Ferla, “SNAP: The SACLANTCEN normal-mode acoustic propagation model,” SACLANT Undersea Research Centre, La Spezia, Italy, 1979.
[18]E. K. Westwood, C. T. Tindle, and N. R. Chapman, “A normal mode model for acoustoelastic ocean environments,” J. Acoust. Soc. Am. **100**, 3631–3645 (1996).
[19]S. E. Dosso, P. L. Nielsen, and M. J. Wilmut, “Data error covariance in matched-field geoacoustic inversion,” J. Acoust. Soc. Am. **119**, 208–219 (2006).
[20]C.-F. Huang, P. Gerstoft, and W. S. Hodgkiss, “Uncertainty analysis in matched-field geoacoustic inversions,” J. Acoust. Soc. Am. **119**, 197–207 (2006).
[21]Y.-M. Jiang and N. R. Chapman, “Quantifying the uncertainty of geoacoustic parameter estimates for the New Jersey Shelf by inverting air gun data,” J. Acoust. Soc. Am. **121**, 1879–1894 (2007).
[22]S. M. Kay, *Fundamentals of Statistical Signal Processing—Volume I: Estimation Theory* (Prentice-Hall, NJ, 1993).
[23]S. Julier, J. Uhlmann, and H. F. Durrant-White, “A new method for nonlinear transformation of means and covariances in filters and estimators,” IEEE Trans. Autom. Control **45**, 477–482 (2000).
[24]A. Doucet, N. de Freitas, and N. Gordon, *Sequential Monte Carlo Methods in Practice* (Springer, New York, 2001).
[25]K. Becker, S. Rajan, and G. Frisk, “Results from the geoacoustic inversion techniques workshop using modal inverse methods,” IEEE J. Ocean. Eng. **28**, 331–341 (2003).
[26]J. Dettmer, S. E. Dosso, and C. W. Holland, “Uncertainty estimation in seismo-acoustic reflection travel time inversion,” J. Acoust. Soc. Am. **122**, 161–176 (2007).
[27]M. Siderius, C. H. Harrison, and M. B. Porter, “A passive fathometer technique for imaging seabed layering using ambient noise,” J. Acoust. Soc. Am. **120**, 1315–1323 (2006).
[28]J.-P. Hermand and P. Gerstoft, “Inversion of broad-band multitone acoustic data from the yellow shark summer experiments,” IEEE J. Ocean. Eng. **21**, 324–346 (1996).
[29]B. Ristic, S. Arulampalam, and N. Gordon, *Beyond the Kalman Filter, Particle Filters for Tracking Applications* (Artech House, Boston, 2004).
[30]H. L. van Trees, *Detection, Estimation and Modulation Theory* (J Wiley, New York, 1968).
[31]M. Zanolin, I. Ingram, A. Thode, and N. C. Makris, “Asymptotic accuracy of geoacoustic inversions,” J. Acoust. Soc. Am. **116**, 2031–2042 (2004).
[32]W. Xu, A. B. Baggeroer, and C. D. Richmond, “Bayesian bounds for matched-field parameter estimation,” IEEE Trans. Signal Process. **52**, 3293–3305 (2004).
[33]C. Yardim, P. Gerstoft, and W. S. Hodgkiss, “Estimation of radio refractivity from radar clutter using Bayesian Monte Carlo analysis,” IEEE Trans. Antennas Propag. **54**, 1318–1327 (2006).
[34]C. Yardim, P. Gerstoft, and W. S. Hodgkiss, “Statistical maritime radar duct estimation using a hybrid genetic algorithm—Markov chain Monte Carlo method,” Radio Sci. **42**, 1–15 (2007).
[35]D. Tollefsen and S. E. Dosso, “Geoacoustic information content of horizontal line array data,” IEEE J. Ocean. Eng. **32**, 651–662 (2007).
[36]Y. Bar-Shalom, X. R. Li, and T. Kirubarajan, *Estimation with Applications to Tracking and Navigation* (Wiley, New York, 2001).
[37]S. McGinnity and G. W. Irwin, “Multiple model bootstrap filter for maneuvering target tracking,” IEEE Trans. Aerosp. Electron. Syst. **36**, 1006–1012 (2000).
[38]T. Schön, F. Gustafsson, and P.-J. Nordlund, “Marginalized particle filters for mixed linear/nonlinear state-space models,” IEEE Trans. Signal Process. **53**, 2279–2289 (2005).
[39]E. A. Wan and R. van der Merve, “The unscented Kalman filter,” in *Kalman Filtering and Neural Networks*, edited by S. Haykin (Wiley, New York, 2001).
[40]N. J. Gordon, D. J. Salmond, and A. F. M. Smith, “Novel approach to nonlinear/non-Gaussian Bayesian state estimation,” IEE Proc. F, Radar Signal Process. **140**, 107–113 (1993).
[41]J. J. K. Ó Ruanaidh and W. J. Fitzgerald, *Numerical Bayesian Methods Applied to Signal Processing*, Statistics and Computing Series (Springer-Verlag, New York, 1996).
[42]P. Tichavský, C. H. Muravchik, and A. Nehorai, “Posterior Cramér-Rao bounds for discrete-time nonlinear filtering,” IEEE Trans. Signal Process. **46**, 1386–1396 (1998).
[43]C. Yardim, P. Gerstoft, and W. S. Hodgkiss, “Tracking refractivity from clutter using Kalman and particle filters,” IEEE Trans. Antennas Propag. **56**, 1058–1070 (2008).